Subregion volume complexity under thermal and electromagnetic quenches

Mohammad Ali-Akbari[*] and Mahsa Lezgi[†]

Department of Physics, Shahid Beheshti University, 1983969411, Tehran, Iran

We study the evolution of holographic subregion complexity (HSC) in a thermally and magnetically quenched, strongly coupled, quantum field theory in $2+1$ dimension. We illustrate two concepts of complexity in this theory: (1) how much information it takes to specify a state by studying the behavior of the final value of HSC in terms of the final temperature and magnetic field and (2) how long it takes to reach the state, by considering the time it takes for HSC to relax as a function of the final temperature and magnetic field. In the first concept, we observe that the effect of temperature and magnetic field on HSC decreases until the energy of the probe is comparable to the final temperature and magnetic field. We present an argument based on an ensemble of microstates corresponding to a given mixed macrostate. In the second concept, we show that the time of relaxation of HSC decreases with the increase of temperature and magnetic field for fixed values of the energy of the probe. We also compare the time evolution of HSC for two quenches in the first concept. We observe that the absolute value of the ratio of the final value of HSC for two kinds of quenches depends on the energy of the probe.

I. INTRODUCTION

Studying the evolution of out-of-equilibrium systems as they move towards equilibrium is a crucial aspect of physics. When these systems are both far from equilibrium and strongly coupled, they become considerably more complex to investigate. To address such nonperturbative problems, including far-from-equilibrium phenomena, one of the tools that physicists have employed is the gauge-gravity duality, or the holographic idea. This duality as a useful framework maps strongly coupled field theories to weakly coupled gravity in one more dimension [1]. A noteworthy example of a strongly coupled and far-from-equilibrium medium is the quark-gluon plasma (QGP) generated during heavy ion collisions at the Relativistic Heavy Ion Collider (RHIC). Experimental observations have revealed that the timescale required for this plasma to reach thermal equilibrium is significantly shorter than what perturbative methods would predict [2].

Such thermalization processes are discussed in the subject of holographic thermalization. One of the ways that a far-from-equilibrium state is prepared is that a limited duration source in time is activated in the boundary field theory. Prior to activating the source, the system exists in its ground sate. The external source performs work on the system, causing it to reach an excited state. This excited state undergoes temporal evolution and eventually, upon deactivating the source, settles into a thermal equilibrium state. The representation of this process on the gravity side is encoded in the process of the formation of a black hole in the bulk [3]. A thermal quench in the boundary theory corresponds to the collapsing of a shell of uncharged matter to anti–de Sitter (AdS) space-time and formation of a Schwarzschild black hole. An electromagnetic quench can be dual to the addition of a shell of charged matter to AdS space-time and the formation of an extremal dyonic black hole [4], as reviewed in this paper. Time evolution of this far-from-equilibrium system can be probed by local and nonlocal observations, and the HSC is the probe we are interested in here.

The holographic concept establishes a connection between quantum information theory quantities and specific geometric quantities in the bulk theory. For instance, the Hubney-Rangamani-Takayanagi (HRT) proposal, which utilizes entanglement entropy as a measure of quantum correlation in a pure quantum state, serves as a straightforward geometric approach [5] that has passed numerous tests successfully [6–14]. Complexity, a fundamental concept in quantum information theory, is defined as the minimum number of simple gates required to generate a given state from a reference state [15]. This quantity refers to the time and space resources needed to perform a computation efficiently [16]. In the realm of quantum field theory, complexity pertains to the minimum

[*]m_aliakbari@sbu.ac.ir
[†]s_lezgi@sbu.ac.ir

number of unitary operators needed to transform a reference state into a target state [17]. Essentially, complexity can be used to classify different quantum states based on the difficulty of their preparation. Within the holographic framework, two conjectures have been proposed to describe complexity: the CV (complexity = volume) conjecture and the CA (complexity = action) conjecture. The complexity in the CA conjecture is determined by evaluating the bulk action on the Wheeler–de Witt patch, which is anchored at a specific boundary time. On the other hand, in the CV conjecture, complexity is defined as the volume of a codimensional-one hypersurface in the bulk that terminates on a time slice of the boundary [18,19]. Initially introduced for the complexity of pure states in the entire boundary system, both conjectures can be extended to encompass the complexity of mixed states in corresponding subregions [20,21]. Inspired by the Hubney-Ryu-Takayanagi proposal, the CV proposal extends to encompass subregions, corresponding to the complexity of mixed states, and is referred to as HSC, in which the complexity of a subsystem on the boundary is determined by the volume of a codimensional-one hypersurface enclosed by a Hubney-Ryu-Takayanagi surface [21]. Numerous studies exploring the CV and CA conjectures, as well as HSC for various gravity models, can be found in the literature [22–34]. It is worth noting that in quantum systems several approaches have been introduced to ensure that the definition of complexity for mixed states does not depend on arbitrary degrees of freedom and can be reduced to the definition of complexity for pure states through purification, such as the spectrum, purification, and ensemble approaches [35]. As a result, various interpretations of HSC also emerge, and the best interpretation has not yet been provided. The description we are using here is that HSC serves as a criterion for quantifying the amount of information required to specify a particular mixed state. In other words, it indicates how difficult it is to generate and specify that mixed state.

In this paper we study the evolution of HSC on a far-from-equilibrium state, under a thermal and an electromagnetic quench for a $2 + 1$ strongly coupled quantum field theory. The evolution of HSC under a thermal quench was first studied in [36]. The new result here is the study of this evolution at zero temperature under a magnetic quench. We try to present the results with a newer perspective compared to what has been done so far, and we compare the results for two types of quench with each other. We numerically calculate the final value of HSC and the relaxation time, the time it takes for HSC to reach a constant value, as the system moves towards equilibrium. We focus on the effect of the energy of the probe, which is characterized by the length of the subregion considered in the boundary as the given mixed state, on the behavior of HSC. Our idea is that in the study of quenched systems holographically, we can highlight two distinct concepts of complexity introduced in the quantum information

literature [16], that is, how much information it takes to specify a state and how many operations are required to reach the state. The final value of HSC as a function of temperature and magnetic field can represent the first concept, and the relaxation time may indicate the second one. We start with a short review on the backgrounds in Sec. II and then compute the HSC in Sec. III and discuss its behavior with numerical results in Sec. IV.

II. REVIEW ON THE BACKGROUND

In this section we review the time-dependent asymptotically AdS_4 geometries corresponding to a thermal and electromagnetic quenched quantum field theory. Holographically, a quench in a quantum field theory can be represented as the collapse of a thin shell of null dust falling from the AdS boundary to form a black hole. This phenomenon can be effectively described using the Vaidya-AdS metric. The metric of the Vaidya-AdS$_4$ can be written as follows [3],

$$ds^2 = \frac{1}{z^2}(-f(z,v)dv^2 - 2dzdv + d\vec{x}^2). \quad (1)$$

The coordinate v labels the path of the ingoing null trajectory and aligns with the time coordinate t on the boundary as z approaches zero. Note that z is the radial coordinate, $\vec{x} \equiv (x_1, x_2)$, and the AdS radius is set to be one. For the thermal quench in which collapsing of an uncharged source leads to the formation of an AdS$_4$-Schwarzschild black hole at late times, corresponding to a thermal state in the dual boundary quantum field theory, we have

$$f(z,v) = 1 - \left(\frac{z}{z_0(v)}\right)^3, \quad m(v) = z_0(v)^{-3}, \quad (2)$$

where $m(v)$ is the mass function of the infalling shell. The subsequent functional form is considered for $z_0(v)$ [37],

$$z_0(v) = z_\infty \left(\frac{1 + \tanh(v/v_0)}{2}\right)^{-1/3}, \quad (3)$$

in which v_0 characterizes the thickness of the shell or the duration of the quench. The parameter z_∞ can be understood as being connected to the final temperature of the background in the late time regime [37],

$$T = \frac{3}{4\pi} z_\infty^{-1}. \quad (4)$$

It is possible to study a completely different type of quench in this system. This nonthermal quench is achieved by introducing electric and magnetic sources in the theory. To ensure a fully nonthermal system, we approach the extremal (zero temperature) black hole

solution at late times [37]. The electric components at late times correspond to nonzero charge density and chemical potential in the dual $2+1$ dimensional boundary quantum field theory [38], while the magnetic components correspond to a background magnetic field [39]. Considering the presence of the electric-magnetic duality invariance of the four dimensional gravity system, different choices of electric or magnetic sources can be interchanged, and for convenience, it is often considered that the systems are undergoing a purely magnetic quench. In this case, the function f is taken to be [37]

$$f(z, v) = 1 - 4\left(\frac{z}{z_0(v)}\right)^3 + 3\left(\frac{z}{z_0(v)}\right)^4. \quad (5)$$

The same quench profile for $z_0(v)$, Eq. (3), is chosen, and this time the parameter z_∞ determines the final strength of the magnetic field [37],

$$B = \sqrt{3}z_\infty^{-2}. \quad (6)$$

We use the metric (1) with (2) and (5) for the thermal and electromagnetic quenches, respectively, to discuss time evolution of the HSC. In order to further study these backgrounds and examine holographic entanglement entropy in them, we refer to Ref. [37].

III. HOLOGRAPHIC SUBREGION COMPLEXITY

The mixed state's complexity, which corresponds to a subregion A on the boundary, is linked to the volume contained by the extremal surface γ_A that appears in the computation of holographic entanglement entropy by the HRT proposal [21], i.e.,

$$\mathcal{C}_A = \frac{V_{\gamma_A}}{8\pi R G_N}, \quad (7)$$

where R, G_N, and $\mathcal{C}_A$ are the AdS radius, Newton's constant, and the HSC for the subregion A, respectively. To calculate γ_A at a given time, we take into account subregion A, which has been defined as

$$A := x_1 (\equiv x) \in \left(-\frac{l}{2}, \frac{l}{2}\right), \qquad x_2 \in \left(-\frac{L}{2}, \frac{L}{2}\right), \quad (8)$$

describing a strip surface of finite length l and width $L \to \infty$ as shown in Fig. 1 for a static AdS background. In general, γ_A does not live on a constant slice for a dynamical background. Due to the symmetry of the strip, it is possible to represent γ_A in the bulk using this parametrization,

$$v = v(x), \quad z = z(x), \quad v\left(\pm\frac{l}{2}\right) = t - \epsilon, \quad z\left(\pm\frac{l}{2}\right) = \epsilon,$$
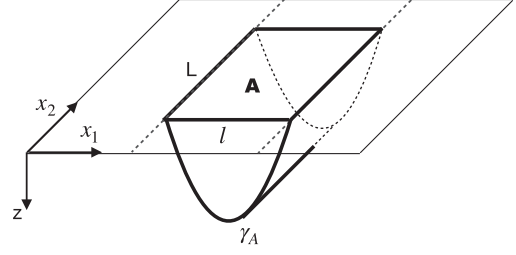$$(9)$$

FIG. 1. Strip entangling surface of length l and width $L \to \infty$ in a static AdS geometry.

where ϵ is a UV cutoff. Then, the area of the minimal surface is obtained easily using Eq. (1),

$$S = \frac{L}{4G_N} \int_{-\frac{l}{2}}^{\frac{l}{2}} \frac{\sqrt{1 - f(z, v)v'^2 - 2z'v'}}{z^2} dx. \quad (10)$$

We treat the integrand in Eq. (10) as a Lagrangian, and the symmetry of the strip causes the turning point of the extremal surface, γ_A, located at $x = 0$, in which

$$v'(0) = z'(0) = 0, \qquad v(0) = v_*, \qquad z(0) = z_*. \quad (11)$$

The equations of motion for $z(x)$ and $v(x)$ can be determined; subsequently, by employing (11), they can be solved numerically to obtain the profiles $z(x)$ and $v(x)$. The volume can be parametrized by $v = v(x)$ and $z = z(x)$, or equivalently $z = z(v)$. According to [40], this x-independent ansatz is, in general, a good approximation just at early and late times. Furthermore, for a small subregion length $l \ll 1/T$, this ansatz provides a good approximation at intermediate times, too. In the following we discuss results in these regions. Therefore, the volume for the background solution (1)—by choosing an appropriate function f [(2) and (5)] for the thermal and electromagnetic quenches, respectively—becomes

$$V = 2L \int_{v_*}^{v\left(\frac{l}{2}\right)} \left(-f(z(v), v) - 2\frac{\partial z}{\partial v}\right)^{\frac{1}{2}} z(v)^{-3} x(v) dv. \quad (12)$$

Since the HSC is divergent, it is convenient to consider subtracted HSC (a normalized version of HSC) using (7), as follows:

$$C \equiv \frac{8\pi R G_N (\mathcal{C} - \mathcal{C}_{\text{AdS}})}{L} = \frac{V - V_{\text{AdS}}}{L}, \quad (13)$$

where $\mathcal{C}$ and $\mathcal{C}_{\text{AdS}}$ are the HSC for A in (1) and AdS geometry, respectively. The volumes are defined with respect to the same boundary region such that V in Eq. (12) reduces to V_{AdS} by setting f equal to one.

To determine the relaxation time for HSC, we introduce the following function:

$$\epsilon(t) = \left| 1 - \frac{C(t)}{C(\infty)} \right|. \qquad (14)$$

The relaxation time t_{eq} is the time at which $\epsilon(t) < 10^{-3}$, and it remains below this limit forever. We will perform numerical calculation for this timescale later.

IV. NUMERICAL RESULTS

We present our results from a numerical calculation of HSC with the metric (1), for both the thermal and electromagnetic quenches. It seems that our holographic calculation shows two distinct concepts of complexity: how much information it takes to specify a state and how many operations are required to reach the state or, in other words, how long it takes to reach the state. A given state can be simple or complex based on these two categories [41]. We plot the final value of HSC, C_{eq}, meaning C at $t \to \infty$, and relaxation time t_{eq}, the time it takes for HSC to relax, in terms of the final temperature and magnetic field to illustrate the two concepts of complexity. On the one hand, the increase or decrease of C_{eq}, due to the amount of information needed to specify the final state by increasing temperature or magnetic field, indicates the first category. On the other hand, the increase or decrease of t_{eq} characterizes the second concept.

In Fig. 2, we show the behavior of C_{eq} as a function of the final temperature. In agreement with our previous argument [42–44], we expect that C_{eq} decreases with the increase of temperature because, with the rise of temperature, the number of microstates corresponding to the mixed macrostate we considered increases. At zero temperature and entropy, a unique configuration corresponding to one microstate requires more information to be specified, but with the increase of the number of microstates, it is not necessary to know the details of the underlying system to specify the macrostate. Therefore, the higher the final temperature, the less information required. However, we notice that this observation depends on the size of the
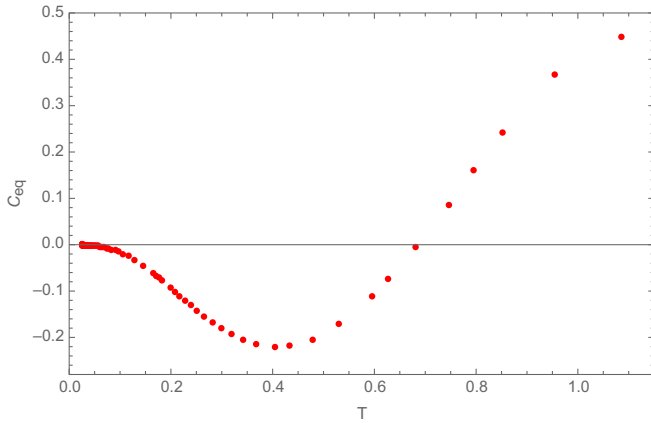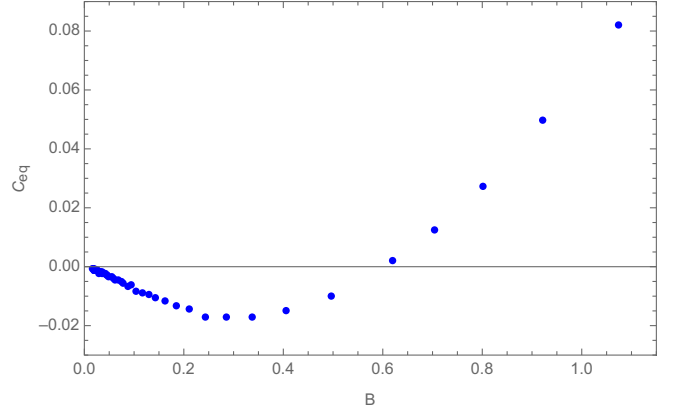

FIG. 3. Plot of C_{eq} in terms of B for $v_0 = 0.01$ and $l = 1.4$.

probe, l. As shown in Fig. 2, C_{eq} starts to increase from the temperature of $T \sim E_l(\equiv \frac{1}{l})$, when the energy of the probe, E_l, is comparable to the final temperature. In the limit of $T \gg E_l$, which means large values of T with fixed E_l or small values of E_l with fixed T, we expect that the degrees of freedom at widely separated scales are largely decoupled from each other. As a result, the HSC practically probes the
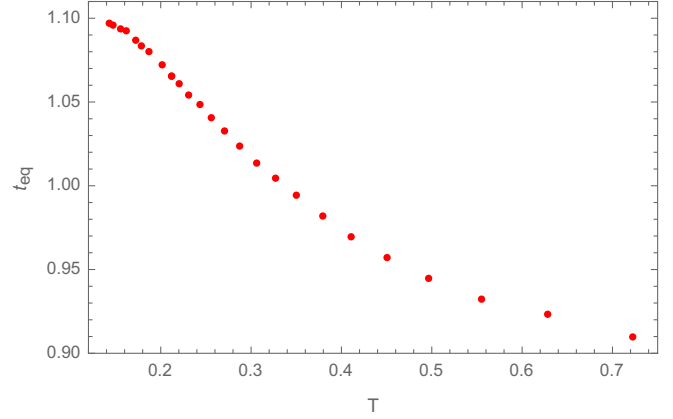

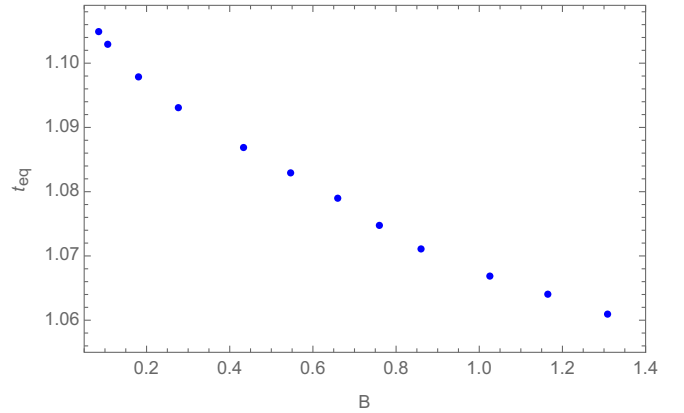FIG. 4. Plot of t_{eq} as a function of T for $v_0 = 0.01$ and $l = 1.4$.

FIG. 2. Plot of C_{eq} as a function of T for $v_0 = 0.01$ and $l = 1.4$.

FIG. 5. Plot of t_{eq} as a function of B for $v_0 = 0.01$ and $l = 1.4$.

zero temperature limit of the field theory, and thus C_{eq} increases, by decreasing E_l or increasing T.

When a magnetic field is applied, the magnetic moments can lower their entropy by becoming magnetized, and thus with the increase of the magnetic field, the entropy tends to decrease. However, in some cases, such as in a QGP plasma, thermodynamic variables like entropy increase with the magnetic field (see Ref. [45] and references therein). Considering that we are also examining QGP-like systems, we expect that C_{eq} would decrease with the increase of the magnetic field since entropy or the number of microstates corresponding to the mixed macrostate
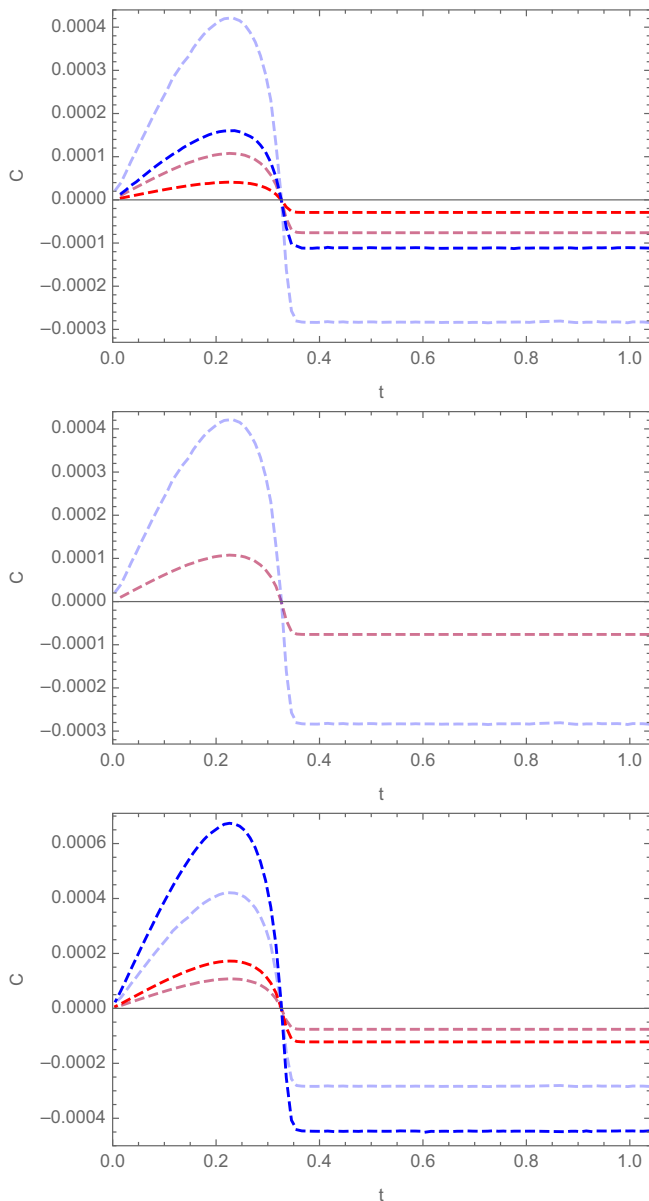
increases. This behavior is shown in Fig. 3. However, similar to the thermal case, there is a stage where C_{eq} increases because E_l is comparable to $\sqrt{B}$. In fact, when $\sqrt{B} \gg E_l$, our probe realizes the $B \to 0$ limit corresponding to a unique configuration or zero entropy and hence leads to higher complexity.

We plot t_{eq} as a function of the final temperature, Fig. 4, and in terms of the final magnetic field, Fig. 5. In both cases, t_{eq} decreases with the increase of temperature and magnetic field. When $T \geq E_l$ ($\sqrt{B} \geq E_l$) our probe investigates the state with a length scale l, associated with E_l, which is larger than the intrinsic length of the theory, $l_T \equiv \frac{1}{T}$ ($l_B \equiv \frac{1}{\sqrt{B}}$). Thus, the precision of the probe is not enough to study scales smaller than l_T (l_B). Therefore, the probe, in the limit of $T(\sqrt{B}) \to \infty \gg E_l$, reports that the temperature (magnetic field) is equal to $T(B)$, and thus, in this limit in which the scales of T ($\sqrt{B}$) and E_l are widely separated, $t_{eq} \to 0$. As a result, by increasing the temperature (magnetic field) for a fixed value of E_l, t_{eq} decreases. To check our argument, we consider the opposite limit. In the limit of $T(\sqrt{B}) \to 0 \ll E_l$ or equivalently $l \ll l_T(l_B)$, as the probe

FIG. 6. Plot of C as a function of t for $B < T$ (top), $B = T$ (middle), and $B > T$ (bottom). Red curves and blue curves show the behavior of C for thermal and electromagnetic quenches, respectively. In the three panels, $l = 0.5$ and $v_0 = 0.01$.
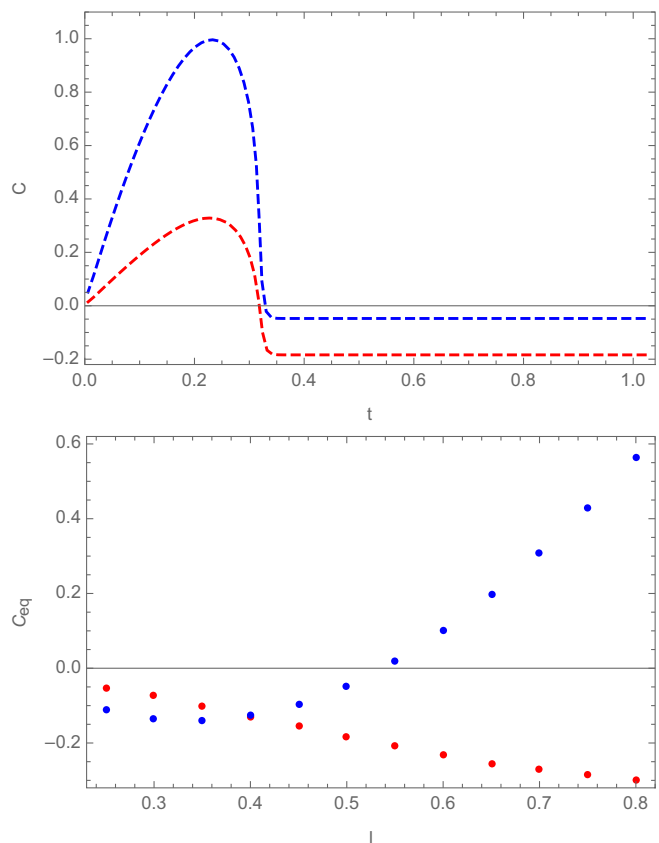

FIG. 7. Top: C as a function of t for $B \gg T$, $l = 0.5$, and $v_0 = 0.01$. The red curve indicates a thermal quench, and the blue one is for an electromagnetic quench. Bottom: C_{eq} in terms of l for a thermal quench (red) and an electromagnetic quench (blue), for $B \gg T$ and $v_0 = 0.01$.

examines the system with more precision, t_{eq} increases in agreement with our argument.

In order to compare two different kinds of quenches, we plot C as a function of time for a thermal quench (red curves) and an electromagnetic quench (blue curves) in Fig. 6. By introducing C_T and C_B as C_{eq} in thermal and electromagnetic quenches, respectively, we list the results as follows:

  (i) $B = T$: The final temperature in a thermal quench is chosen to be equal to the final magnetic field in an electromagnetic quench. In the middle panel of Fig. 6, we observe that $C_B < C_T$.

 (ii) $B < T$: The final magnetic field is chosen to be smaller than the final temperature. In the top panel of Fig. 6, we observe that $C_B < C_T$ and $|C_B - C_T|$ are smaller than in the case of $B = T$.

(iii) $B > T$: The final magnetic field is chosen to be larger than the final temperature. In the bottom panel of Fig. 6, we observe that $C_B < C_T$ and $|C_B - C_T|$ are larger than in the case of $B = T$.

In the second and third categories, the temperature and magnetic field differences have been chosen to be the same, and in all categories, we observe that $C_B < C_T$. As we explained earlier, both an increase in temperature in the thermal system and an increase in the magnetic field in the electromagnetic system at zero temperature increase the entropy or, equivalently, increase the number of microstates and thus reduce the complexity. The reason why $C_B < C_T$ might be intuitively related to the fact that a thermal system has statistical fluctuations and is a statistical system, whereas an electromagnetic system at zero temperature is deterministic and predictable. Note that the reliability of this statement depends on E_l. We can highlight it by considering $B \gg T$ or $T \gg B$ limits, as we discuss next.

In the top panel of Fig. 7, we plot C in terms of time for $B \gg T$. In this case, as shown in the bottom panel of Fig. 7, whether C_B is smaller or larger than C_T depends on the length of the subregion, l. For small enough values of l, $C_B < C_T$. However, for large enough l or, in other words, small enough energy of the probe, E_l, $C_B > C_T$. This behavior is consistent with the results shown in Fig. 3, where C_B starts to increase for large B or small E_l, as we explained before. Note that C_T also starts to increase with the increase of l, but it happens at larger l values than in the electromagnetic case because $B \gg T$. According to this explanation, we can predict the case of $T \gg B$ as well, in which, for small enough values of l, $C_T < C_B$, and then for large values of l, $C_B < C_T$. However, due to the limitations of numerical calculations, we have not plotted it here.
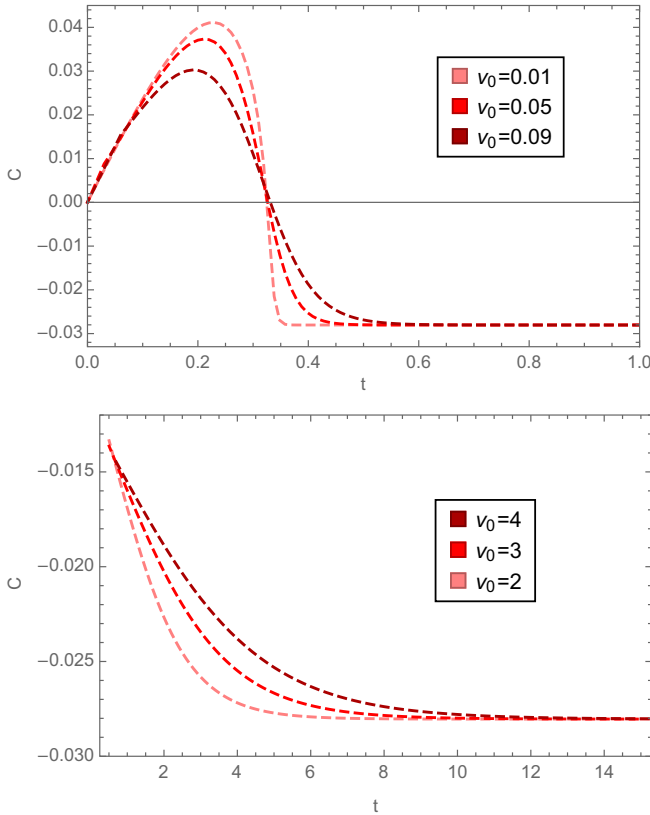

FIG. 8. Plot of C as a function of t at $l = 0.5$ and $T = 0.238$ for three values of v_0 in the range of fast quenches (top) and slow quenches (bottom).
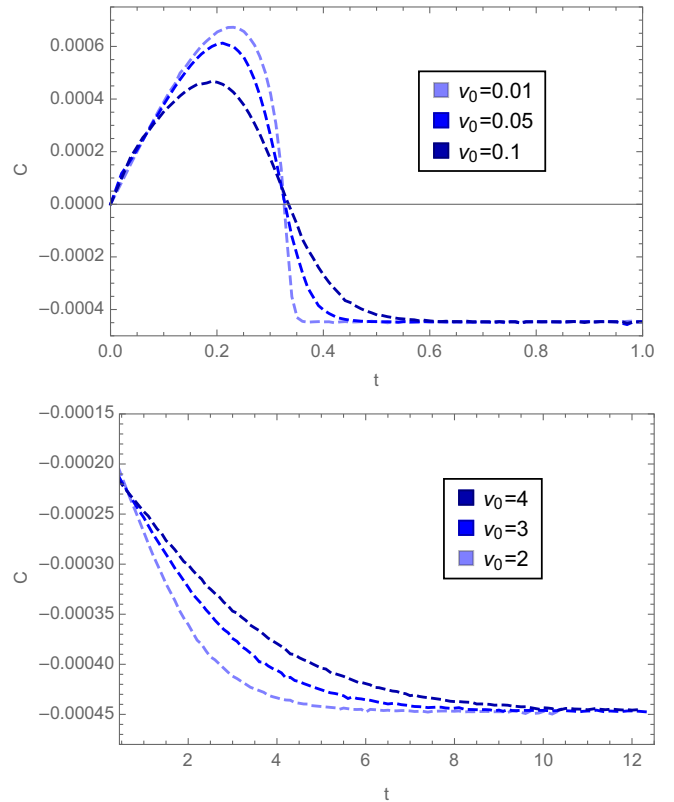
FIG. 9. Plot of C as a function of t at $l = 0.5$ and $B = 0.045$ for three values of v_0 in the range of fast quenches (top) and slow quenches (bottom).

We would like to mention that these results for the zero temperature case under a magnetic quench can be compared to the result for holographic complexity for the pure thermofield state in the zero temperature limit. In that case, unlike the results of HSC here, the complexity rate vanishes in this limit [46]. Therefore, it could be said that HSC seems to probe rather different physics compared to the complexity of the whole system [47].

To study the effect of the parameter v_0 (which is considered as the speed of the quench in the boundary field theory) on the evolution of the HSC, we plot C in terms of time for three values of v_0 in both fast and slow quenches, for a thermal quench in Fig. 8 and the electromagnetic case in Fig. 9. In a fast quench, the system rapidly changes, while in a slow quench, the system undergoes an adiabatic transition and has enough time to equilibrate during the evolution. In a fast quench, the HSC experiences an increase at the early stage, reaches a maximum value, and then decreases to C_{eq} at late times. As can be seen in both figures, different manners of energy injection into the system result in different responses during early time intervals. Hence, by knowing only about T or B in the boundary field theory, the HSC can distinguish between fast and slow quenches. We have seen this behavior before for a different model [42]. Furthermore, the faster the

energy injection, the earlier the system reaches HSC equilibrium. Therefore, in a fast quench, the system reaches equilibrium earlier than a slow quench for both thermal and electromagnetic quenches. The top panels of Figs. 8 and 9 show that for thermal and electromagnetic quenches, respectively, with the increase of v_0 in the range of fast quenches, the maximum value of HSC becomes smaller and is reached sooner, and the system achieves HSC equilibrium later. The bottom panels of Figs. 8 and 9 show that for thermal and electromagnetic quenches, respectively, with the increase of v_0 in the range of slow quenches, the system reaches HSC equilibrium later.

Finally, it is worth noting that in [48], the evolution of the circuit complexity for a subsystem in harmonic lattices after a global quantum quench of the mass parameter has been calculated. Interestingly, this evolution depicts a local maximum before the saturation regime, which is a feature that has been observed for HSC in Vaidya gravitational backgrounds, like in this work.

ACKNOWLEDGMENTS

[1] J. Casalderrey-Solana, H. Liu, D. Mateos, K. Rajagopal, and U. A. Wiedemann, *Gauge/String Duality, Hot QCD and Heavy Ion Collisions* (Cambridge University Press, Cambridge, England, 2014).

[2] R. Baier, A. H. Mueller, D. Schiff, and D. T. Son, Bottom up thermalization in heavy ion collisions, Phys. Lett. B **502**, 51 (2001).

[3] V. Balasubramanian, A. Bernamonti, J. de Boer, N. Copland, B. Craps. E. Keski-Vakkuri, B. Muller, A. Schafer, M. Shigemori, and W. Staessens, Thermalization of strongly coupled field theories, Phys. Rev. Lett. **106**, 191601 (2011).

[4] A. Chamorro and K. S. Virbhadra, A radiating dyon solution, Pramana **45**, 181 (1995).

[5] Veronika E. Hubney, Mukund Rangamani, and Tadashi Takayanagi, A covariant holographic entanglement entropy proposal, J. High Energy Phys. 07 (2007) 062.

[6] Mukund Rangamani and Tadashi Takayanagi, Holographic entanglement entropy, Lect. Notes Phys. **931**, 1 (2017).

[7] Parul Jain, Siddhi Swarupa Jena, and Subhash Mahapatra, Holographic confining-deconfining gauge theories and entanglement measures with a magnetic field, Phys. Rev. D **107**, 086016 (2023).

[8] Roldao da Rocha, Holographic entanglement entropy, deformed black branes, and deconfinement in AdS/QCD, Phys. Rev. D **105**, 026014 (2022).

[9] David Dudal and Subhash Mahapatra, Interplay between the holographic QCD phase diagram and entanglement entropy, J. High Energy Phys. 07 (2018) 120.

[10] Zhibin Li, Kun Xu, and Mei Huang, The entanglement properties of holographic QCD model with a critical end point, Chin. Phys. C **45**, 013116 (2021).

[11] Irina Ya. Aref'eva, Alexander Patrushev, and Pavel Slepov, Holographic entanglement entropy in anisotropic background with confinement-deconfinement phase transition, J. High Energy Phys. 07 (2020) 043.

[12] Parul Jain and Subhash Mahapatra, Mixed state entanglement measures as probe for confinement, Phys. Rev. D **102**, 126022 (2020).

[13] M. Ali-Akbari and M. Lezgi, Holographic QCD, entanglement entropy, and critical temperature, Phys. Rev. D **96**, 086014 (2017).

[14] M. Rahimi, M. Ali-Akbari, and M. Lezgi, Entanglement entropy in a non-conformal background, Phys. Lett. B **771**, 583 (2017).

[15] John Watrous, Quantum computational complexity, arXiv: 0804.3401.

[16] Micheal A. Nielsen and Isaac L. Chuang, *Quantum Computation and Quantum Infromation* (Cambridge University Press, Cambridge, England, 2010), p. 702.

[17] R. Jefferson and R. C. Myers, Circuit complexity in quantum field theory, J. High Energy Phys. 10 (2017) 107.

[18] D. Stanford and L. Susskind, Complexity and shock wave geometries, Phys. Rev. D **90,** 126007 (2014).

[19] A. R. Brown, D. A. Roberts, L. Susskind, B. Swingle, and Y. Zhao, Complexity, action, and black holes, Phys. Rev. D **93,** 086006 (2016).

[20] Dean Carmi, Robert C. Myers, and Pratik Rath, Comments on holographic complexity, J. High Energy Phys. 03 (2017) 118.

[21] Mohsen Alishahiha, Holographic complexity, Phys. Rev. D **92,** 126009 (2015).

[22] Omer Ben-Ami and Dean Carmi, On volumes of subregions in holography and complexity, J. High Energy Phys. 11 (2016) 129.

[23] S. J. Zhang, Complexity and phase transitions in a holographic QCD model, Nucl. Phys. **B929,** 243 (2018).

[24] S. J. Zhang, Subregion complexity in holographic thermalization with dS boundary, Eur. Phys. J. C **79,** 715 (2019).

[25] Pratim Roy and Tapobrata Sarkar, On subregion holographic complexity and renormalization group flows, Phys. Rev. D **97,** 086018 (2018).

[26] R Fareghbal and P Karimi, Complexity growth in flat spacetimes, Phys. Rev. D **98,** 046003 (2018).

[27] M. Alishahiha, A. Faraji Astaneh, M. R. Mohammadi Mozaffar, and A. Mollabashi, Complexity growth with Lifshitz scaling and hyperscaling violation, J. High Energy Phys. 07 (2018) 042.

[28] M. Alishahiha, K. Babaei Velni, and M. R. Mohammadi Mozaffar, Subregion action and complexity, Phys. Rev. D **99,** 126016 (2019).

[29] Mahsa Lezgi and Mohammad Ali-Akbari, A note on holographic subregion complexity and QCD phase transition, Phys. Rev. D **101,** 026022 (2020).

[30] M. asadi, On volume subregion complexity in non-conformal theories, Eur. Phys. J. C **80,** 681 (2020).

[31] Mahsa Lezgi, Mohammad Ali-Akbari, and Mohammad Asadi, Non-conformality, subregion complexity and meson binding, Phys. Rev. D **104,** 026001 (2021).

[32] Andrew R. Frey, Michael P. Grehan, and Manu Srivastava, Complexity of scalar collapse in anti-de Sitter spacetime, J. High Energy Phys. 12 (2021) 135.

[33] Juan Hernandez, Robert C. Myers, and Shan-Ming Ruan, Quantum extremal islands made easy. Part III. Complexity on the brane, J. High Energy Phys. 02 (2021) 173.

[34] Yi Ling, Yuxuan Liu, Chao Niu, Yikang Xiao, and Cheng-Yong Zhang, Holographic subregion complexity in general Vaidya geometry, J. High Energy Phys. 11 (2019) 039.

[35] Cesar A. Agon, Santa Barbara, Matthew Headrick, and Brian Swingle, Subsystem complexity and holography, J. High Energy Phys. 02 (2019) 145.

[36] Bin Chen, Wen-Ming Li, Run-Qiu Yang, Cheng-Yong Zhang, and Shao-Jun Zhang, Holographic subregion complexity under a thermal quench, J. High Energy Phys. 07 (2018) 034.

[37] Tameem Albash and Clifford V. Johnson, Evolution of holographic entanglement entropy after thermal and electromagnetic quenches, New J. Phys. **13,** 045017 (2011).

[38] Andrew Chamblin, Roberto Emparan, Clifford V. Johnson, and Robert C. Myers, Charged AdS black holes and catastrophic holography, Phys. Rev. D **60,** 064018 (1999).

[39] Sean A. Hartnoll and Pavel Kovtun, Hall conductivity from dyonic black holes, Phys. Rev. D **76,** 066001 (2007).

[40] Roberto Auzzi, Giuseppe Nardelli, Fidel l. Schaposnik Massolo, Gianni Tallarita, and Nicolo Zenoni, On volume subregion complexity in Vaidya spacetime, J. High Energy Phys. 11 (2019) 098.

[41] Leonard Susskind, Entanglement is not enough, Fortschr. Phys. **64,** 49 (2016).

[42] Mahsa Lezgi and Mohammad Ali-Akbari, Complexity and uncomplexity during energy injection, Phys. Rev. D **103,** 126024 (2021).

[43] Mohammad Ali-Akbari and Mahsa Lezgi, Note on stability and holographic subregion complexity, Eur. Phys. J. C **82,** 114 (2022).

[44] Mohammad Ali-Akbari and Mahsa Lezgi, Resource and stability near a critical point from the quantum information perspective, Phys. Lett. B **842,** 137954 (2023).

[45] Yogesh. Kumar, Effect of magnetic field on QGP equation of state, J. Phys. Soc. Jpn. Conf. Proc. **26,** 024028 (2019).

[46] Dean Caemi, Shira Chapman, Hugo Marrochio, Robert C. Myers, and Sotaro Sugishita, On the time dependence of holographic complexity, J. High Energy Phys. 11 (2017) 188.

[47] We would like to thank the referee for a comment on this point.

[48] Giuseppe Di Giulio and Erik Tonni, Subsystem complexity after a global quantum quench, J. High Energy Phys. 05 (2021) 022.